

Morphotectonics of the Raman-Panikkar-Wadia seamount chain in the Laxmi Basin, Eastern Arabian Sea

**J. John Savio^{a,b}, V. Yatheesh^{a,*}, C.M. Bijesh^c, K. Mahender^b, K.K. Aswini^a,
Firoz Badesab^a, M. Shuhail^{a,c}, G. Sriram^a, D. Twinkle^a, Raj Kumar^a**

^aCSIR - National Institute of Oceanography, Dona Paula, Goa 403 004, India

^bSchool of Earth, Ocean and Atmospheric Sciences, Goa University,
Taleigao Plateau, Goa 403 206, India

^cNational Centre for Polar and Ocean Research, Ministry of Earth Sciences,
Vasco da Gama, Goa 403 804, India

* Corresponding author

E-mail address: yatheesh@nio.org; yatheeshv@gmail.com (V. Yatheesh)

Tel: +91 832 2450563

Abstract

The Laxmi Basin, which is a deep ocean basin situating adjoining to the northwestern continental margin of India, contains a linear seamount chain consisting of the Raman Seamount, Panikkar Seamount and the Wadia Guyot, located over the axial basement high in the Laxmi Basin representing the Panikkar Ridge. The geomorphology of this seamount chain was studied by earlier researchers; however, its characteristic geophysical signatures, possible genesis and age of formation remains to be clearly established. We attempted for a detailed understanding of the morphological characteristics and the geophysical signatures over the spatial extent of these seamounts using a fresh set of multibeam bathymetry data and sea-surface gravity and magnetic anomalies, complemented by the existing seismic reflection sections. Based on the seafloor and basement topography signatures observed together from the multibeam bathymetry data and the seismic reflection sections, we infer that all the three seamounts are associated with the presence of surface/subsurface secondary peaks on their central parts. The free-air gravity anomaly maps show that the seamounts are associated with a very short wavelength gravity high, superimposed on the short wavelength gravity low representing the Panikkar Ridge. The magnetic anomaly maps suggest that all these seamounts are associated with complex magnetic signatures. Based on the presence of morphological features that are generally associated with the volcanic activity and by considering the above complex geophysical signatures and the updated magnetic isochron map of the Laxmi Basin, we support multiphased volcanic origin for the Raman-Panikkar-Wadia seamount chain, emplaced at an age younger to 63.28 Ma.

Key words: Seamounts; Laxmi Basin; Morphology, Tectonics, Volcanism

1. Introduction

The Laxmi Basin represents the deep offshore region existing between the northwestern continental margin of India and the NW-SE trending segment of the Laxmi Ridge (Fig. 1). The published hydrographic chart and a regional bathymetric profile collected during the SK50 expedition onboard ORV Sagar Kanya revealed the presence of a chain of seamounts in the axial part of the Laxmi Basin. The detailed bathymetric investigation of these seamounts was originally carried out by Bhattacharya et al. (1994b) using the swath bathymetric data collected during the SK79 expedition onboard *RV Sagar Kanya* in 1992, and brought out geomorphology of this seamount chain consisting of three seamounts, referred to as the Raman Seamount, the Panikkar Seamount and the Wadia Guyot, from north to south (Fig. 1). These seamounts represent three isolated bathymetric highs located over the quasi-linear NNW-SSE trending basement high zone, referred to as the Panikkar Ridge (Gopala Rao et al., 1992). The seafloor morphology of these features were depicted by Bhattacharya et al. (1994b) as two-dimensional contour maps and three-dimensional mesh surface diagrams. During the last three decades, several new data analyses techniques have been developed to better understand the morphology of the various seafloor features using the gridded data. However, due to the unavailability of the digital gridded data used for the above study, such modern analyses could not be performed. In addition, several improvements have also occurred in the acquisition of high-resolution multibeam bathymetry data. Further, Bhattacharya et al. (1994b) restricted their investigation only to the seafloor morphology of these seamounts and no other geophysical characteristics such as gravity and magnetic signatures as well as the sub-seafloor characteristics were studied. Such an understanding is important to decipher the detailed morphotectonics and early evolution of the Arabian Sea and the adjoining northwestern continental margin of India that can also provide important insights on the hydrocarbon prospectivity of these regions. Therefore, we carried out a detailed geophysical investigation over these seamounts using a fresh set of high-resolution sea-surface multibeam bathymetry, gravity and magnetic data, complemented with the available seismic reflection profiles.

2. Tectonic framework

The large-scale plate tectonic reconstruction models of the Indian Ocean (Norton and Sclater, 1979; Besse and Courtillot, 1988; Scotese et al., 1988) suggest that the formation of the Arabian Sea commenced at around 63 Ma by seafloor spreading through the Carlsberg Ridge. However, based on the detailed geomagnetic investigation in the deep offshore region existing between the Laxmi Ridge and the northwestern continental margin of India, Bhattacharya et al. (1994a) invoked another episode of seafloor spreading (~84.0 to ~65.0 Ma) prior to the initiation of seafloor spreading through the

Carlsberg Ridge. Subsequently several researchers (Bhattacharya and Yatheesh, 2015; Shuhail et al., 2018; Yatheesh, 2020; Yatheesh et al., 2020) carried out detailed geophysical investigations on these regions and provided stage-by-stage plate tectonic reconstruction model by accommodating this inferred episode of seafloor spreading in the Laxmi Basin (Fig. 2). According to these revised plate tectonic reconstruction models, the plate tectonic evolution of the western continental margin of India and its adjacent deep offshore regions were evolved due to the rifting and drifting among the Southern Indian Protocontinent (SIP), Northern Indian Protocontinent (NIP), Seychelles Plateau (SEY), Madagascar (MAD), Laxmi Ridge (LAX) and the Laccadive Plateau (LCP). This model suggests that the plate tectonic evolution of the Arabian Sea occurred in three stages. The first stage was the rifting of Madagascar from the combined SIP-NIP-LAX-LCP-SEY block, which began at around 88 Ma (Fig. 2a). This breakup was initiated when this region came in the proximity of the Marion hotspot, causing widespread volcanism on the conjugate sides of Madagascar (Storey et al., 1995; Torsvik et al., 1998; Torsvik et al., 2000) and India (Valsangkar et al., 1981; Radhakrishna et al., 1994; Radhakrishna et al., 1999; Torsvik et al., 2000; Anilkumar et al., 2001; Pande et al., 2001; Melluso et al., 2009; Radhakrishna and Joseph, 2012; Ram Mohan et al., 2016; Sheth et al., 2017). Soon after this, seafloor spreading between Madagascar and SIP-NIP-LAX-LCP-SEY block was initiated resulting in the formation of the Mascarene Basin (Fig. 2b). The second stage was the rifting and drifting of SIP, NIP, and the conjoint SEY-LAX blocks through the Gop-Narmada-Laxmi Triple Junction, which commenced at around 68.5 Ma (Fig. 2c). The relative motion among these blocks developed the Laxmi Basin between the Southern Indian Protocontinent and the NW-SE trending segment of the Laxmi Ridge; the Gop Basin between the E-W trending segment of the Laxmi Ridge and the Saurashtra Volcanic Platform (which forms a part of the Northern Indian Protocontinent), and the Narmada Rift Graben between the Southern and Northern Indian protocontinental blocks (Fig. 2c). The presence of 68.5 Ma old volcanics, representing the earliest pulse of the Réunion hotspot (Basu et al., 1993), located north of the major Deccan Flood Basalt Province, has been used to constrain the timing of initiation of rifting across the arms of the Gop-Narmada-Laxmi Triple Junction. Concurrently, another axis of divergence emerged between SIP and LCP, which lead to the formation of the Laccadive Basin (Yatheesh et al., 2020). The third stage was the separation of LAX and SEY blocks, which began at around 63 Ma by the seafloor spreading at the Carlsberg Ridge, resulting in the formation of the Arabian Basin on the Laxmi Ridge side, and its conjugate Eastern Somali Basin on the Seychelles side (Fig. 2d). The timing of this breakup is constrained by the inferred age of the oldest magnetic lineations (Miles and Roest, 1993; Chaubey et al., 2002) from the Arabian and Eastern Somali basins following the geomagnetic polarity reversal timescale of Cande and Kent (1995). The formation and evolution

of the Laxmi Basin and its axial seamount chain are considered to have formed during the second and third stages of the plate tectonic evolution of the Arabian Sea.

3. Data and methodology

The main data used in the present study consists of the high-resolution multibeam bathymetry data, and sea-surface magnetic and gravity profiles acquired during the SSD-030 and SSD-073 expeditions conducted onboard *RV Sindhu Sadhana* by the CSIR – National Institute of Oceanography, Goa, India. The multibeam bathymetry data was collected using Teledyne-Atlas multibeam echo sounders, operated at a frequency of 15 kHz, to understand the seafloor morphology of the seamounts and the adjoining regions in 1000 m to 4000 m depth range. The measured depth values are corrected for variation of sound velocity in seawater by collecting sound velocity profiles in real-time. This raw multibeam dataset was processed using Teledyne PDS software (version 4.4). Finally, manual de-spiking and qualitative filtering were applied to minimise the erroneous depth soundings. The processed data was extracted in ASCII format and prepared the bathymetric grid with 100 m spatial resolution. All of the shipboard multibeam bathymetric maps presented in this study were generated with this gridded data. For various morphometric calculations, we used Generic Mapping Tools (Wessel et al., 2019) and the Mirone (Luis, 2007) softwares. For analysing the multibeam bathymetry data to map the gully patterns around the seamounts, we used Geographical Information System (QGIS version 3.22, <https://qgis.org>) platform. To understand the sub-seafloor characteristics of these seamounts, we used seismic reflection data acquired during AAS-09 expedition onboard *RV AAS Sidorenko* by the CSIR – National Institute of Oceanography, Goa, India. In addition, we used a part of the published (Krishna et al., 2010) seismic section along the profile RE-11 that cut across the Wadia Guyot. Shipboard BGGs Gravimeter KSS 32-M was used to acquire sea-surface gravity data and was then reduced to gravity anomalies by applying Normal and Eötvös corrections. The closely spaced criss-crossing tracks were used for the generation of detailed shipborne free-air anomaly grids of the three seamounts, after applying cross-over corrections. A self-oscillating split-beam Geometrics-882 Cesium Vapour marine magnetometer was used for sea-surface magnetic data acquisition. These data were reduced to residual magnetic anomalies by applying International Geomagnetic Reference Field (IGRF) for the corresponding epoch. As in the case of gravity anomalies, the closely spaced criss-crossing tracks were used for the generation of detailed shipborne magnetic anomaly grids of the three seamounts, after applying cross-over corrections. The locations of the multibeam bathymetry, sea-surface gravity, magnetic and seismic-reflection profiles used in the present study are given in Fig. 3.

4. Results and Discussions

4.1 Seafloor morphology from multibeam bathymetry data

We present various maps to depict the morphological characteristics of the Raman Seamount, the Panikkar Seamount and the Wadia Guyot using the newly acquired high-resolution multibeam bathymetry data. These maps include high-resolution bathymetric maps represented as two-dimensional (Fig. 4) and three-dimensional (Fig. 5) images, slope maps (Figs. 6a-c), terrain aspect maps (Figs. 6d-f), terrain ruggedness maps (Figs. 6g-i), and channel pattern maps (Fig. 7). The 2-D and 3-D bathymetric images (Figs. 4 and 5) provide detailed information on the spatial variation of the seafloor topography, which in turn, were used to delineate the various seafloor features defined by the elevations and depressions on the seafloor. The map showing the spatial variations of the slope (Figs. 6a-c), which defines the measure of the steepness, have been used to identify the sharp drops/rises on the seafloor. The terrain aspect (Figs. 6d-f) has been used to represent the measured angle showing the orientation in which the seamounts are exposed. The ruggedness index (Riley et al., 1999) have been used to understand the distribution of terrain heterogeneity (Figs. 6g-i) by calculating the change in elevation between a grid cell and its 3×3 neighbour cells that represents a measure of the local variation in seabed terrain in the oceanic areas (Wilson et al., 2007). The channel pattern maps (Fig. 7) have been used to identify and delineate the various dendritic gully patterns all around the seamounts.

4.1.1 The Raman Seamount

The bathymetric maps (Figs. 4a, 5a, and Supplementary Fig. S1) show that the Raman Seamount is an elliptical and elongated feature, which is trending approximately in the N-S direction (azimuth direction ~40). This seamount rises from the surrounding flat seafloor with an average water depth of about 3550 m. The southwestern flank of the seamount is ~ 30-40m deeper than its northeastern flank. The elongated primary mount with a basal area of ~665 km² rises up to ~2474 m. The seamount upsurges with steep lower flanks up to a depth of about 2850-2750 m. The upper portion of this region is less steep and areas having water depths shallower than 2600 m forms a relatively flat plateau. A secondary peak is present over the plateau, with its base at a depth of ~2500 m. The secondary peak with a basal area of ~25 km² comes across its summit at ~2042 m water depth, giving the total height of the seamount as ~1507 m. At ~2550 m level, the plateau appears to give rise to a ridge-like feature which is somewhat in a concave shape facing toward the east, along the long axis of the seamount. The 3-D images of the seamount (Fig. 5a and Supplementary Fig. S1) indicates that this ridge-like feature is situated slightly towards the western part of the plateau and, therefore, divides the plateau asymmetrically. The Raman Seamount is also associated with several distinct channel pattern and the

associated dendritic erosional gullies on its primary peak (Fig. 7a). The morphometric parameters of the Raman Seamount derived from the present study are given in the Table 1.

The slope map of the Raman Seamount (Fig. 6a) shows that the seamount is represented by closed boundaries of the primary and secondary peaks, and in general, these peaks are defined by the slope values ranging between $\sim 10^\circ$ and $\sim 35^\circ$, with the steepest slopes ($> 50^\circ$) coinciding with the sharp erosional gullies. The Terrain Aspect map of the Raman Seamount (Fig. 6d) shows that a hinge line divides the seamount longitudinally to two asymmetric parts, the west-facing (defined by red-shaded region) and east-facing (defined by blue-shaded region) flanks. The location of this hinge line coincides with the ridge-like feature that is situated over the Raman Seamount as observed from the 3-D bathymetric map (Fig. 5a). From the relative ruggedness map (Fig. 6g), it is observed that the most rugged regions of the Raman Seamount are associated with steep erosional gullies and the least rugged regions are the top portion of the relatively flat area within the primary peak of the Raman Seamount.

4.1.2 The Panikkar Seamount

The bathymetric maps (Figs. 4b, 5b, and Supplementary Fig. S2) of the Panikkar Seamount show the presence of three bathymetric highs that make up an elongated arcuate shape. These three bathymetric highs are referred to as the Segment-1 (S1), Segment-2 (S2) and Segment-3 (S3) of the Panikkar Seamount, from northwest to southeast, respectively, following Savio et al. (2022). The segments S1 and S2 are built on a single platform and are connected by a linear, narrow, steeply sloped ridge-like feature, while the segment S3 is a small, isolated feature from the main platform of the Panikkar Seamount, separated by a flat seafloor. Both the segments, S1 and S2, exhibit a steep drop in depth on the western boundary, but towards the east and south, these features exhibit a comparatively smooth topography. The highest peak of the Panikkar Seamount is at ~ 2618 m and is situated on S1 (near $16^\circ 13'N$). The 3-D maps (Figs. 5b, and Supplementary Fig. S2) of this crescent-shaped peak shows a nearly southward deepening structure similar to a flank collapse / crater-wall collapse of a previously active volcanic structure. Debris lobes observed on the foot of this inferred steeply dipping structure (Fig. 5b, Supplementary Fig. S2) further support a possible slope failure / flank collapse. In addition, the Panikkar Seamount is associated with several volcanic caldera-like features, as reported by Savio et al. (2022), supporting the volcanic origin for this seamount. The Panikkar Seamount is also associated with several distinct channel pattern and the associated dendritic erosional gullies on all the three segments (Fig. 7b). A major, nearly N-S trending channel pattern observed on this map coincides with the location of the southward deepening structure inferred to represent a flank collapse / crater-wall collapse. The morphometric parameters of the Panikkar Seamount derived from the present study are given in the Table 1.

The slope map of the Panikkar Seamount (Fig. 6b) shows that the seamount is represented by nearly closed boundaries of the segment S1 (except around the inferred collapse structure) and the ridge-like feature connecting the segments S1 and S2, with a hinge line observed along this ridge-like feature. In general, the boundary of the Panikkar Seamount is defined by the slope values ranging between $\sim 10^\circ$ and $\sim 30^\circ$. The terrain aspect map of the Panikkar Seamount (Fig. 6e) shows that a hinge line divides the seamount longitudinally into two asymmetric parts, a narrower west-facing (defined by red-shaded region) flank and a wider east-facing (defined by blue-shaded region) flank. From the relative ruggedness map (Fig. 6h), it is observed that the most rugged regions of the Panikkar Seamount are associated with steep erosional gullies.

4.1.3 The Wadia Guyot

The Wadia Guyot represents the southernmost seamount in the Laxmi Basin axial seamount chain. This flat-topped seamount is the largest in this seamount chain. The multibeam bathymetry maps (Figs. 4c, 5c, and Supplementary Fig. S3) reveal that the Wadia Guyot is an elongated elliptical feature trending in the \sim NNW-SSE direction, which is nearly identical to the general trend of the direction of the seamount chain. The seamount rises from the surrounding flat seafloor with an average water depth of about 3700 m. This seamount is ~ 2365 m high from the surrounding seafloor. The Wadia Guyot is represented by a secondary flat-topped feature (defined by ~ 1600 m and 1446 m isobaths) that covers an area of ~ 134 sq. km, which is located over a primary flat-topped feature (defined by ~ 2100 m and ~ 1900 m isobaths). The bathymetry data of the Wadia Guyot further reveals the presence of several volcanic cones on its northern as well as the south-southeastern parts. The Wadia Guyot is also associated with several distinct channel pattern and the associated dendritic erosional gullies on its primary as well as secondary peaks (Fig. 7c). The morphometric parameters of the Wadia Guyot derived from the present study are given in the Table 1.

The slope map (Fig. 6c) shows that the eastern and western sides of the primary peak of the Wadia Guyot are characterised by linear steep-slope regions, with their maximum slope coinciding with the locations of erosional gullies. However, the southern and the northern boundaries of this feature are not bounded by any such steep-slope regions. Rather, these regions are characterized by the presence of flanks dipping gently away from the summit region. The secondary peak of the Wadia Guyot is associated with a closed boundary defined by slope values ranging between $\sim 15^\circ$ and $\sim 35^\circ$. The terrain aspect map of the Wadia Guyot (Fig. 6f) shows a gradual variation of the terrain aspect from east to west without any distinct hinge line as in the case of Raman and Panikkar seamounts. From the relative ruggedness map (Fig. 6i), it is observed that the most rugged regions of the Wadia Guyot are associated

with steep erosional gullies, especially on its eastern flank and the least rugged regions are the top portion of the relatively flat area within the secondary peak of the Wadia Guyot.

4.2 Seafloor and sub-seafloor topography from seismic sections

The published seismic reflection sections (Srinivas, 2004; Krishna et al., 2006; Corfield et al., 2010; Krishna et al., 2010; Misra et al., 2016; Pandey et al., 2020; Nair et al., 2021) in the Laxmi Basin and the surrounding regions reveal the presence of several NNW-SSE trending seafloor and basement features, which mainly consists of the Laxmi Ridge, the Panikkar Ridge and the Raman-Panikkar-Wadia seamount chain. We present the seismic sections (Fig. 8) that cut across the Raman Seamount (along the profile AS09-04a), the Panikkar Seamount (along the profile AS09-10a) and the Wadia Guyot (along the profile RE-11a), depicting the seafloor and basement topography.

The seismic section along the profile AS09-04a (Fig. 8a, b), traversing the Raman Seamount (profile location in Fig. 3) shows the presence of a broad topographic high in the seafloor with maximum relief of ~2.2 seconds of two-way travel time (TWT). This topographic feature, which is with a thickness of ~1.25 seconds TWT, has ~22 km width at the base on the seafloor and ~15 km width at its summit of the major feature. The summit region of the seamount is covered by about 0.4 - 0.6 seconds (TWT) of the thick acoustically transparent sediment layer. The acoustic basement topography of this region, as interpreted by Srinivas (2004), reveals that the Raman Seamount is characterised by relatively steeply dipping flanks, with onlap of sediments on its eastern and western flanks. The seismic section along the profile AS09-04a (Figs. 8a, b) further shows an ~4 km wide secondary topographic high with a relief of ~0.6 seconds TWT over the primary topographic structure of the Raman Seamount.

The seismic section along the profile AS09-10a (Figs. 8c, d), cutting across the Segment S1 of the Panikkar Seamount (profile location in Fig. 3), shows that the seamount is nearly conical as defined by the seafloor and basement topography interpreted by Srinivas (2004). This seismic section shows that the highest relief of the Panikkar Seamount occurs at ~1.2 seconds TWT from the surface. The primary feature of the Segment S1 is ~15 km wide as defined at the seafloor and has a summit width of ~8 km. On top of this summit (Segment S1 of the Panikkar Seamount), there exists a ~0.5 Seconds (TWT) thick acoustically transparent sediment layer. This seismic section also reveals the presence of a subsurface secondary basement peak analogous to the secondary peak of the Raman Seamount, although this inferred secondary peak over the Panikkar Seamount is buried under the sediments unlike the Raman Seamount. Such an observation of the presence of secondary peak over the Panikkar Seamount further corroborates the multiphase volcanism occurred in the Segment S1 region of the Panikkar Seamount postulated by Savio et al. (2022). The acoustic basement topography along the

profile AS09-10a shows that the Panikkar Seamount is associated with steeply dipping flanks with onlap of sediments on both flanks, as in the case of the Raman Seamount.

The only published seismic section available across the Wadia Guyot is along the profile RE-11 (Krishna et al., 2006; Krishna et al., 2010). We present a part of this seismic section (RE-11a) across the Wadia Guyot (profile location in Fig. 3) to depict the seafloor and basement topography of this anomalous feature. It is important to note that the profile RE-11a is located further north of the flat-topped summit region of the Wadia Guyot and therefore the flat-topped seafloor, that is used to classify this anomalous feature as a guyot, is not evidenced in this section. The Wadia Seamount, which has a width of ~30 km at the seafloor, is covered by about 0.8 seconds (TWT) thick sediment layer. As in the case of the Raman and Panikkar seamounts, the Wadia Guyot also is associated with steeply dipping flanks with onlap of sediments. The central part of the Wadia Guyot is characterized by the presence of an intrusive body that is associated with bulging of the sediments. Such an observation possibly indicates the multiphase volcanism occurred at a later stage of its formation and evolution.

4.3 Gravity signatures

The geophysical investigations in the northwestern continental margin of India and the adjoining regions (Naini, 1980; Naini and Talwani, 1982; Bhattacharya et al., 1994a; Krishna et al., 2006; Yatheesh, 2007) revealed that the Laxmi Basin is characterised by a broad gravity high with a superimposed short-wavelength gravity low in its axial part representing the Panikkar Ridge, over which the Raman-Panikkar-Wadia seamounts are situated. To characterize the gravity signatures of the Raman Seamount, Panikkar Seamount, and the Wadia Guyot, we present free-air gravity anomaly maps (Fig. 9 and Supplementary Fig. S4) prepared using the free-air gravity anomaly grids derived from all the available ship tracks (Fig. 3) across these seamounts. The free-air gravity anomaly map of the Raman Seamount (Fig. 9a), with the superimposed bathymetry contours, shows that the gravity anomalies are well correlatable with the topography, with their maximum (~20 mGal) located over the summit of this seamount. These gravity anomalies decrease along the flanks of the features and get superimposed on the gravity signature of the surrounding nearly flat seafloor. The gravity anomaly map further suggests that the western flank of the seamount buried under the sediments is relatively gentle compared to the eastern flank. As a result, the extent of the seamount defined by the basement topography in the western side of the seamount is further westward than the extent defined by the seafloor topography, while in the eastern side, the extent of the basement high is relatively closer to the extent of the seamount defined by the seafloor topography. The free-air gravity anomaly map of the Panikkar Seamount (Fig. 9b), with the superimposed bathymetry contours, shows that the gravity anomalies are well correlatable with the topography, with their maximum (~5 mGal) centred around

the peak of Segment S1 of the Panikkar Seamount. The free-air gravity anomalies decrease from the summit through the flanks and get superimposed on the gravity minimum over the surrounding flat seafloor. It is further observed that the free air gravity anomaly of the western flank is relatively gentle when compared to the eastern flank of the seamount. The free-air gravity anomalies of the Wadia Guyot (Fig. 9c), with the superimposed bathymetry contours, are well correlatable with the topography, with their free-air gravity anomaly maximum (~ 44 mGal) located on the plateau over the guyot. The flat-topped summit region shows an overall characteristic gravity high zone and these anomalies decrease along the flanks of the features and get superimposed on the gravity signature of the surrounding flat seafloor. The eastern and western boundaries of the Wadia Guyot defined by the maximum slope of the free-air gravity anomalies (representing the base of the basement feature) nearly coincide with the respective bathymetric extent at the seafloor. This observation suggests that both the flanks of the Wadia Guyot are associated with nearly vertical flanks, unlike the Raman and Panikkar Seamount.

4.4 Magnetic signatures

To characterize the magnetic signatures of the Raman Seamount, Panikkar Seamount, and the Wadia Guyot, we present magnetic anomaly maps (Fig. 10 and Supplementary Fig. S5) prepared using the magnetic anomaly grids derived from all the available ship tracks (Fig. 3) across these seamounts. The magnetic anomaly map of the Raman Seamount (Fig. 10a), with the superimposed bathymetry contours, shows that the seamount is associated with negative magnetic anomalies in major part of this seamount. The gradual variation of the magnetic anomalies from negative to positive representing the inflection point is located near the latitude around $17^{\circ}12'N$. The northern tip of the Raman Seamount is associated with a positive magnetic anomaly that form a part of the large positive magnetic anomaly band observed in the region north of the Raman Seamount. In the major part of the eastern boundary of the Raman Seamount, the negative to positive transition of the magnetic anomalies occurs along the region coinciding with the bathymetric boundary of the seamount. The magnetic anomaly map (Fig. 10b) shows that the Panikkar Seamount is associated with a complex magnetic signature. The northern half of the segment S1 of the Panikkar Seamount is characterized by a negative magnetic anomaly while the segments S2, S3 and the southern half of S1 are associated with positive magnetic signatures. The magnetic anomaly maximum is observed in the southern part of the segment S2 and the segment S3. An isolated magnetic high is observed in the southeastern part of segment S1, and interestingly, this magnetic high coincide with the location of the largest caldera-like feature identified by Savio et al. (2022). The magnetic anomaly map of the Wadia Guyot (Fig. 10c), with the superimposed bathymetry contours, shows that the seamount is associated with a complex magnetic signature. The

major part of the Wadia Guyot, existing between latitudes 15°25'N and 15°45'N, is associated with negative magnetic anomaly. Northward of 15°45'N and southward of 15°25'N, gradual transition occurs from negative to positive magnetic anomalies. In the northwestern part of the Wadia Guyot, the transition of negative to positive anomaly occurs along the region coinciding with the boundary of the seamount defined by bathymetry contours. The southernmost and northwestern parts of the Wadia Guyot is bounded by a semi-circular band of magnetic anomaly high.

4.5 Probable genesis and age of formation of the seamount chain

The Raman Seamount, Panikkar Seamount, and the Wadia Guyot, together considered as a seamount chain, are located in the axial part of the Laxmi Basin. Difference in opinion exists about the genesis of these seamounts. Some researchers (Krishna et al., 2006; Geoffroy et al., 2020) considered them as isolated highs of thinned continental crust / isolated continental block (C-block), forming a part of the Panikkar Ridge. Conversely, others (Bhattacharya et al., 1994b; Bhattacharya and Yatheesh, 2015; Misra et al., 2015; Pande et al., 2017; Pandey et al., 2020; Savio et al., 2022) considered these seamounts to have formed by volcanism. Bhattacharya et al. (1994b) attributed the genesis of these seamounts to an episode of volcanism due to the intersection of extinct spreading centre and the hotspot, considering the similar trends of the seamount chain and the volcanic trail of the proximal Réunion hotspot. Bhattacharya and Yatheesh (2015) later supported this inference by estimating the location of the Réunion hotspot based on the updated plate tectonic reconstruction depicting the early opening of the Arabian Sea, and inferred an age of ~62.5 Ma for the formation of this seamount chain considering the relationship between the location and extent of the seamounts with the location of the mapped magnetic isochrons. Misra et al. (2015) interpreted these seamounts as isolated and sub-rounded volcanic cones based on the analysis of high-resolution multichannel seismic reflection sections. From the analysis of seismic reflection profiles, Nemčok et al. (2016) inferred that the Panikkar Ridge, over which the seamount chain situates, is formed by a volcanic plug. Based on the geochronological investigations on the Ghatkopar-Powai volcanics and comparing those results with the published offshore tectonic inferences of Bhattacharya and Yatheesh (2015) derived from marine magnetic investigations, Pande et al. (2017) inferred that the Ghatkopar-Powai volcanics on the Indian mainland and the Raman-Panikkar-Wadia seamount chain in the offshore region were emplaced by nearly contemporaneous volcanic events (Mukherjee et al., 2020). Recently, based on the analysis of the high-resolution multibeam bathymetry data, Savio et al. (2022) identified six semi-circular caldera-like features on the Panikkar Seamount, implying a volcanic origin for this seamount, which forms a part of the Laxmi Basin seamount chain. Based on the presence of primary and secondary peaks, volcanic cones, and crater-like features derived from our bathymetry data, the complex basement

topography with intrusive structures derived from the seismic reflections section and the complex magnetic signatures associated with the seamounts, and in conjunction with the above published inferences, we support volcanic origin for the formation of the seamount chain, caused by multiple phases of volcanism.

Although the geophysical signatures strongly support the volcanic origin of the seamounts, the age of this volcanic episode is yet to be established. In absence of the age information derived from direct geochronological investigations using the rock samples collected from these seamounts, researchers attempted to provide indirect constraints to provide a reasonable explanation for the timing of occurrence of these postulated volcanic events that created this seamount chain. Bhattacharya and Yatheesh (2015) observed that the lateral extents of the main edifices of the seamount chain are restricted within the basement younger than chron C28no, implying that the formation of seamounts were younger to 63.6 Ma (based on the geomagnetic polarity reversal timescale of Cande and Kent (1995)). Subsequently, based on the geochronological investigation using $^{40}\text{Ar}/^{39}\text{Ar}$ dating, Pande et al. (2017) estimated an age of ~62.5 Ma for the Ghatkopar-Powai volcanics (forming a part of the Deccan volcanics) and considered the formation of these onshore volcanics to be contemporaneous to the volcanic episode that lead to the formation of the Raman-Panikkar-Wadia seamount chain in the offshore region, considering the inference of Bhattacharya and Yatheesh (2015). However, Pandey et al. (2020) assigned an age of 65.5 Ma for the formation of this seamount chain based on regional geology and seismic constraints.

It may be noted that the magnetic isochrons mapped by Bhattacharya and Yatheesh (2015) that were used to infer the age of formation for this seamount chain was limited only to four magnetic anomaly picks around the Raman Seamount, and three magnetic anomaly picks around the Panikkar Seamount. Since we acquired more number of closely spaced magnetic anomaly profiles, we attempted to map these magnetic lineations around the seamount chain in larger spatial resolution by extending the identifications of Bhattacharya and Yatheesh (2015) on these newly acquired magnetic profiles. While extending these identifications on new profiles, we also reassigned the age of the magnetic anomalies using the latest available geomagnetic polarity reversal timescale of Malinverno et al. (2020). This updated magnetic isochron map (Fig. 11) in better resolution and with reassigned age of this magnetic polarity reversal timescale suggests that the Raman and Panikkar seamounts were emplaced at an age younger to 63.28 Ma (chron C28ny). However, it may be noted that these magnetic lineations of chron C28ny are restricted only near to the Raman and Panikkar seamounts, which are located within the inferred now extinct spreading centre within the extent of the oceanic crust of the Laxmi Basin defined by the presence of linear magnetic anomalies. These magnetic lineations are observed till the southern

part of the Panikkar Seamount, and further southwards, i.e., around the Wadia Guyot, no such lineations are identifiable (Fig. 11a). Such an observation implies two scenarios. The first scenario is that, as in the case of the Raman and Panikkar seamounts, there existed magnetic lineations representing chron C28ny in both the sides of the Wadia Guyot also, and the later phases of Réunion hotspot volcanism in the offshore region might have obliterated these original signatures representing these magnetic anomalies and making these original evidences untraceable. The second scenario is that the southernmost part of the Laxmi Basin, where the Wadia Guyot is located and the magnetic lineations are absent, is associated with rifting only, and the divergence in this region has not reached the stage of rift-drift transition, resulting in the formation of the oceanic crust, unlike in the region near to the Raman and Panikkar Seamounts, where magnetic lineations are mapped. It is interesting to note that this is the region inferred to have been underlain by thinned continental crust intermingled with volcanic intrusives by Krishna et al. (2006) based on the integrated interpretation of geophysical data along the profile RE-11 (see the Fig. 1 of Krishna et al. (2006)) using integrated gravity-magnetic modelling under the seismic constraints. If this interpretation is correct, then the Wadia Guyot might have formed in a different set up (i.e., volcanic intrusion within thinned continental crust formed by rifting) compared to the formation of the Raman and Panikkar seamounts, which were formed on the oceanic crust during the waning phase of seafloor spreading, commencing from chron C28ny (~63.3 Ma). However, detailed investigations in these regions are required to evaluate these propositions and the possibility of explaining the part of the Laxmi Basin where the magnetic lineations are present as oceanic in nature and the southernmost part of the Laxmi Basin, where no magnetic lineations are present as continental in nature.

The Raman Seamount, Panikkar Seamount and the Wadia Guyot are associated with surface / basement topographic highs representing secondary peaks as well as several volcanic cones / caldera-like features as evidenced from the multibeam bathymetry and the seismic sections. These features might represent multiple phases of volcanism occurred during the waning stage of the Laxmi Basin evolution. Such an inference of multiphase volcanism in this region is further supported by the presence of complex magnetic anomalies, some of which are associated with bathymetric / basement topography, while others are not associated with any such features, implying the possible presence of subsurface intrusives.

5. Summary and Conclusions

We carried out a detailed marine geophysical investigation over the seamount chain located in the axial part of the Laxmi Basin to understand their morphology, geophysical characteristics, probable genesis and age of formation. The bathymetric maps prepared using the high-resolution multibeam bathymetry

data suggest that the Raman Seamount is characterized by the presence of an elongated primary bathymetric high over which a secondary peak is situated; the Panikkar Seamount is characterized by an arcuate-shaped anomalous bathymetric high consisting of three segments S1, S2 and S3; and the Wadia Guyot is characterized by the presence of a flat-topped secondary feature lying over an elongated primary bathymetric high. The sub-seafloor topography from the seismic sections shows the presence of relatively steeply-dipping flanks, with onlap of sediments on the eastern and western flanks of all these seamounts. The interpreted basement topography further shows the presence of secondary peaks on the central part of all these three seamounts. The free-air gravity anomaly maps of these seamounts are well correlatable with the topography, with their maxima on the summit regions. For the Wadia Guyot, the free-air gravity anomalies (representing the base of the basement feature) nearly coincide with the respective bathymetric extent at the seafloor, whereas in the case of the Raman and Panikkar seamounts, the subsurface extent is beyond the bathymetric extent defined by the seafloor topography. The magnetic anomaly maps suggest that all the three seamounts are associated with complex magnetic signatures, with their summit regions associated with characteristic negative magnetic anomalies. The northern part of the Raman Seamount, the southeastern part of the Panikkar Seamount and the southernmost and northwestern part of the Wadia Guyot are bounded by bands of magnetic anomaly highs.

The morphological characteristics and the geophysical signatures of the seamount chain strongly support multiphased volcanic origin for the formation of the Raman-Panikkar-Wadia seamount chain. This inference is mainly based on the presence of elongated primary features representing the main edifices of the seamounts, secondary peaks, volcanic cones, and crater-like features derived from the bathymetry data, the complex basement topography with intrusive structures derived from the seismic reflections section, and the complex magnetic signatures associated with the seamounts. Based on the updated magnetic isochrons mapped around these seamounts, and comparing the relationship of the extent of the seamounts with these magnetic lineations, we observed that the Raman and Panikkar seamounts are bounded by the magnetic lineations representing chron C28ny on both the sides, implying that these seamounts were emplaced at an age younger to 63.28 Ma. However, detailed geochronological and geochemical investigations using the rock samples collected from the primary and secondary peaks of these seamounts are required to constrain the age of formation of different parts of the seamounts formed by different phases of volcanism.

Declaration of competing interest

The authors declare that they have no known competing financial interests or personal relationships that could have influenced the work presented in this study.

Acknowledgement

The authors are grateful to Prof. Sunil Kumar Singh, Director, CSIR-National Institute of Oceanography (CSIR-NIO), Goa, India, and Dr. Thamban Meloth, Director, National Centre for Polar and Ocean Research (NCPOR), Goa, India, for granting permission to publish this work. This study forms a part of PhD work of JJS at Goa University. JJS thank Council of Scientific and Industrial Research (CSIR), New Delhi, India, for the financial support under Junior Research Fellowship (Grant No. 31/026(0321)/2019-EMR-I). We are grateful to Mr. Milind Naik, Mr. Kallathian M., Mr. Rebello Sheldon and Mr. Kuldeep Kumar from Research Vessel Management Group of CSIR-NIO for their excellent technical support during the expeditions SSD-030 and SSD-073 onboard *RV Sindhu Sadhana*. The cooperation and support received from the captains and their operational team onboard *RV Sindhu Sadhana* during these expeditions are acknowledged. We are indebted to Prof. Soumyajit Mukherjee and an anonymous reviewer for their careful review of the manuscript and valuable comments. We thank Mr. G.C. Bhattacharya for fruitful discussions and for providing seismic sections along the profiles AS09-04a and AS09-10a, and Dr. K. Srinivas for providing digital data of the interpreted line drawings of the basement identifications along these profiles. We are also grateful to Mr. S. Gautham and Ms. Jeffy Solly John for their help extended for processing the bathymetry data and analysing channel maps, respectively. We used Mirone software (Luis, 2007) to handle the grid data and Generic Mapping Tools (Wessel et al., 2019) to plot all the figures presented in this paper. This is NIO contribution XXXX and NCPOR contribution J-XX/20XX-XX.

References

- Anilkumar, Pande, K., Venkatesan, T.R., Bhaskar Rao, Y.J., 2001. The Karnataka Late Cretaceous dykes as products of the Marion hotspot at the Madagascar - India breakup event: evidence from $^{40}\text{Ar}/^{39}\text{Ar}$ geochronology and geochemistry. *Geophysical Research Letters* 28, 2715-2718.
- Basu, A.R., Renne, P.R., Dasgupta, D.K., Teichmann, F., Poreda, R.J., 1993. Early and late igneous pulses and high ^3He plume origin for the Deccan Flood Basalts. *Science* 261, 902-906.
- Besse, J., Courtillot, V., 1988. Paleogeographic maps of the continents bordering the Indian Ocean since the Early Jurassic. *Journal of Geophysical Research* 93, 11791-11808.
- Bhattacharya, G.C., Chaubey, A.K., Murty, G.P.S., Srinivas, K., Sarma, K.V.L.N.S., Subrahmanyam, V., Krishna, K.S., 1994a. Evidence for seafloor spreading in the Laxmi Basin, northeastern Arabian Sea. *Earth and Planetary Science Letters* 125, 211-220.
- Bhattacharya, G.C., Murty, G.P.S., Srinivas, K., Chaubey, A.K., Sudhakar, T., Nair, R.R., 1994b. Swath bathymetric investigation of the seamounts located in Laxmi Basin, Eastern Arabian Sea. *Marine Geodesy* 17, 169-182.

- Bhattacharya, G.C., Yatheesh, V., 2015. Plate-tectonic evolution of the deep ocean basins adjoining the western continental margin of India - a proposed model for the early opening scenario, In: Mukherjee, S. (Ed.), *Petroleum Geoscience: Indian Contexts*. Springer International Publishing, Switzerland, pp. 1-61.
- Cande, S.C., Kent, D.V., 1995. Revised calibration of the geomagnetic polarity time scale for the Late Cretaceous and Cenozoic. *Journal of Geophysical Research* 100, 6093-6095.
- Chaubey, A.K., Dymant, J., Bhattacharya, G.C., Royer, J.Y., Srinivas, K., Yatheesh, V., 2002. Paleogene magnetic isochrons and palaeo-propagators in the Arabian and Eastern Somali basins, NW Indian Ocean, In: Clift, P.D., Croon, D., Gaedicke, C., Craig, J. (Eds.), *The Tectonic and Climatic Evolution of the Arabian Sea Region*. Geological Society, London, Special Publication 195, pp. 71-85.
- Corfield, R.I., Carmichael, S., Bennett, J., Akhter, S., Fatimi, M., Craig, T., 2010. Variability in the crustal structure of the West Indian Continental Margin in the Northern Arabian Sea. *Petroleum Geoscience* 16, 257-265.
- GEBCO Compilation Group, 2021. GEBCO 2021 Grid; doi:10.5285/c6612cbe-50b3-0cffe053-6c86abc09f8f.
- Geoffroy, L., Guan, H., Gernigon, L., Foulger, G.R., Werner, P., 2020. The extent of continental material in oceans: C-blocks and the laxmi basin example. *Geophysical Journal International*.
- Krishna, K.S., Chaubey, A.K., Gopala Rao, D., Reddy, P.R., 2010. Seismic structure and tectonics of the continental margins of India, In: Reddy, P.R. (Ed.), *Seismic imaging of the Indian Continental and Oceanic crust*. Professional Book Publisher, Hyderabad, pp. 324-432.
- Krishna, K.S., Rao, D.G., Sar, D., 2006. Nature of the crust in the Laxmi Basin (14° - 20°), western continental margin of India. *Tectonics* 25, TC1006, doi:10.1029/2004TC001747.
- Luis, J.F., 2007. Mirone: A multi-purpose tool for exploring grid data. *Computers and Geosciences* 33, 31-41.
- Malinverno, A., Quigley, K.W., Staro, A., Dymant, J., 2020. A Late Cretaceous-Eocene geomagnetic polarity timescale (MQSD20) that steadies spreading rates on multiple mid-ocean ridge flanks. *Journal of Geophysical Research: Solid Earth* 125, e2020JB020034.
- Melluso, L., Sheth, H.C., Mahoney, J.J., Morra, V., Petrone, C.M., Storey, M., 2009. Correlations between silicic volcanic rocks of the St. Mary's Islands (southwestern India) and eastern Madagascar : implications for Late Cretaceous India-Madagascar reconstructions. *Journal of the Geological Society, London* 166, 283-294.
- Miles, P.R., Roest, W.R., 1993. Earliest seafloor spreading magnetic anomalies in the north Arabian Sea and the ocean-continent transition. *Geophysical Journal International* 115, 1025-1031.
- Misra, A.A., Banerjee, S., Kundu, N., Mukherjee, B., 2016. Subsidence around oceanic ridges along passive margins: NE Arabian Sea. *Geological Society, London, Special Publications* 445, 119-149.
- Misra, A.A., Sinha, N., Mukherjee, S., 2015. Repeat ridge jumps and microcontinent separation: insights from NE Arabian Sea. *Marine and Petroleum Geology* 59, 406-428.

- Mukherjee, S., Dole, G., Yatheesh, V., Kale, V.S., 2020. Tectonics of the Deccan Trap: Focus on Indian Geoscientists' Contribution in the Last Four Years. *Proceedings of Indian National Science Academy* 86, 237-244.
- Naini, B.R., 1980. Geological and Geophysical study of the continental margin of Western India, and the adjoining Arabian Sea including the Indus cone. Columbia University, p. 173.
- Naini, B.R., Talwani, M., 1982. Structural framework and the evolutionary history of the continental margin of Western India, In: Watkins, J.S., Drake, C.L. (Eds.), *Studies in continental margin geology*. American Association of Petroleum Geologists, pp. 167-191.
- Nair, N., Pandey, D.K., Pandey, A., Prerna, R., 2021. Seismic stratigraphy and the sedimentation history in the Laxmi Basin of the eastern Arabian Sea: Constraints from IODP Expedition 355. *Geoscience Frontiers* 12, 101111.
- Nemčok, M., Sinha, S.T., Doré, A.G., Lundin, E.R., Mascle, J., Rybár, S., 2016. Mechanisms of microcontinent release associated with wrenching-involved continental break-up; a review. *Geological Society, London, Special Publications* 431, 323-359.
- Norton, I.O., Sclater, J.G., 1979. A model for the evolution of the Indian Ocean and the break-up of Gondwanaland. *Journal of Geophysical Research* 84, 6803-6830.
- Pande, K., Sheth, H.C., Bhutani, R., 2001. $^{40}\text{Ar} - ^{39}\text{Ar}$ age of the St. Mary's Islands volcanics, southern India: record of India - Madagascar break-up on the Indian subcontinent. *Earth and Planetary Science Letters* 193, 39-46.
- Pande, K., Yatheesh, V., Sheth, H., 2017. $^{40}\text{Ar}/^{39}\text{Ar}$ dating of the Mumbai tholeiites and Panvel flexure: intense 62.5 Ma onshore-offshore Deccan magmatism during India-Laxmi Ridge-Seychelles breakup. *Geophysical Journal International* 210, 1160-1170.
- Pandey, D.K., Pandey, A., Clift, P.D., Nair, N., Ramesh, P., Kulhanek, D.K., Yadav, R., 2020. Flexural subsidence analysis of the Laxmi Basin, Arabian Sea and its tectonic implications. *Geological Magazine* 157, 834-847.
- Radhakrishna, T., Dallmeyer, R.D., Joseph, M., 1994. Paleomagnetism and $^{36}\text{Ar}/^{40}\text{Ar}$ vs $^{39}\text{Ar}/^{40}\text{Ar}$ isotope correlation ages of dyke swarms in Central Kerala, India: tectonic implications. *Earth and Planetary Science Letters* 121, 213-226.
- Radhakrishna, T., Joseph, M., 2012. Geochemistry and paleomagnetism of Late Cretaceous mafic dikes in Kerala, southwest coast of India in relation to large igneous provinces and mantle plumes in the Indian Ocean region. *Geological Society of America Bulletin* 124, 240-255.
- Radhakrishna, T., Maluski, H., Mitchell, J.G., Joseph, M., 1999. $^{40}\text{Ar}-^{39}\text{Ar}$ and K/Ar geochronology of the dykes from the south Indian granulite terrain. *Tectonophysics* 304, 109-129.
- Ram Mohan, M.R., Shaji, E., Satyanarayanan, M., Santosh, M., Tsunogae, T., Yang, Q.-Y., Dhanil Dev, S.G., 2016. The Ezhimala Igneous Complex, southern India: Possible imprint of Late Cretaceous magmatism within rift setting associated with India-Madagascar separation. *Journal of Asian Earth Sciences* 121, 56-71.
- Riley, S.J., DeGloria, S.D., Elliot, R., 1999. A terrain ruggedness index that quantifies topographic heterogeneity. *Intermountain Journal of Sciences* 5, 23-27.

- Savio, J.J., Yatheesh, V., Sheldon, R., Kallathian, M., Kessarkar, P., Kumar, K., Mahesh, P., Mishra, S., Verma, S., 2022. Caldera-like features located over the Panikkar Seamount and adjacent regions in the Laxmi Basin, eastern Arabian Sea. *Journal of Earth System Science* 131, 44.
- Scotese, C.R., Gahagan, L.M., Larson, R.L., 1988. Plate tectonic reconstructions of the Cretaceous and Cenozoic ocean basins. *Tectonophysics* 155, 27-48.
- Sheth, H., Pande, K., Vijayan, A., Sharma, K.K., Cucciniello, C., 2017. Recurrent Early Cretaceous, Indo-Madagascar (89–86 Ma) and Deccan (66 Ma) alkaline magmatism in the Sarnu-Dandali complex, Rajasthan: $^{40}\text{Ar}/^{39}\text{Ar}$ age evidence and geodynamic significance. *Lithos* 284–285, 512-524.
- Srinivas, 2004. Seismic reflection and bathymetric study over deep offshore regions off the central west coast of India, Department of Earth Science. Goa University, Goa, p. 180.
- Storey, M., Mahoney, J.J., Saunders, A.D., Duncan, R.A., Kelley, S.P., Coffin, M.F., 1995. Timing of hotspot related volcanism and the breakup of Madagascar and India. *Science* 267, 852-855.
- Torsvik, T.H., Tucker, R.D., Ashwal, L.D., Carter, L.M., Jamtveit, V., Vidyadharan, K.T., Venkataramana, P., 2000. Late cretaceous India - Madagascar fit and timing of breakup related magmatism. *Terra Nova* 12, 220-224.
- Torsvik, T.H., Tucker, R.D., Ashwal, L.D., Eide, E.A., Rakotosolof, N., de Wit, M., 1998. Late Cretaceous volcanism in Madagascar: Paleomagnetic evidence for a stationary Marion hotspot. *Earth and Planetary Science Letters* 164, 221-232.
- Valsangkar, A.B., Radhakrishnamurthy, C., Subbarao, K.V., Beckinsale, R.D., 1981. Paleomagnetism and Potassium-Argon age studies of acid igneous rocks from the St. Mary Islands. *Geological Society of India*, pp. 265-275.
- Wessel, P., Luis, J.F., Uieda, L., Scharroo, R., Wobbe, F., Smith, W.H.F., Tian, D., 2019. The Generic Mapping Tools Version 6. *Geochemistry, Geophysics, Geosystems* 20, 5556-5564.
- Wilson, M.F.J., O'Connell, B., Brown, C., Guinan, J.C., Grehan, A.J., 2007. Multiscale Terrain Analysis of Multibeam Bathymetry Data for Habitat Mapping on the Continental Slope. *Marine Geodesy* 30, 3-35.
- Yatheesh, V., 2007. A study of tectonic elements of the western continental margin of India and adjoining ocean basins to understand the early opening of the Arabian Sea. Goa University, Goa, p. 212.
- Yatheesh, V., 2020. Structure and tectonics of the continental margins of India and the adjacent deep ocean basins: Current status of knowledge and some unresolved problems. *Episodes* 43, 586-608.
- Yatheesh, V., Bhattacharya, G.C., Shuhail, M., 2020. Revised plate tectonic reconstruction model for the early opening of the Arabian Sea, In: Rossi, P., François, C., Miles, P. (Eds.), *The Indian Ocean and its Margins*. Commission for the Geological Map of the World, France, pp. 11-12.

Figure Captions

Fig. 1: (a) Topographic map of the northwestern continental margin of India and the adjoining deep ocean basins as depicted by the GEBCO 2021 global terrain model for ocean and land (GEBCO Compilation Group, 2021), showing the location of the axial seamount chain in the Laxmi Basin. Thin black lines are selected (1000 m., 2000 m., 3000 m., and 4000 m.) bathymetry contours. The inset map shows the location of the study area in the Indian Ocean; (b) Generalized tectonic map of the Laxmi Basin and the adjacent regions showing the magnetic lineations (Bhattacharya and Yatheesh, 2015) as thin black lines, the extent of the Panikkar Ridge (Srinivas, 2004) shown as green shaded region, and the locations of the Raman-Panikkar-Wadia seamount chain (Bhattacharya et al., 1994b) shown as red contours. ABB: Arabian Basin; LXB: Laxmi Basin; LAX: Laxmi Ridge; LCP: Laccadive Plateau; PKR: Panikkar Ridge; R: Raman Seamount; P: Panikkar Seamount; W: Wadia Guyot

Fig. 2: Illustrative representation depicting the major stages of formation and evolution of the western continental margin of India and the adjacent deep ocean basins (modified after Yatheesh (2020), ages are reassigned based on Malinverno et al., 2020). (a) ~88.0 Ma; (b) ~84.0 Ma; (c) ~68.5 Ma; (d) ~63.3 Ma;

Legends: [1] Major continental blocks, [2] Microcontinents, [3] Ultra-thinned continental crust, [4] Volcanics, [5] Location of the Marion Hotspot, [6] Location of the Réunion Hotspot, [7] Rift axis, [8] Ridge axis, [9] Transform fault, [10] Extinct spreading centre/failed rift, [11] Palaeo-transform fault, [12] location of the Gop-Narmada-Laxmi Fossil Triple Junction off the Saurashtra Peninsula. SIP: Southern Indian Protocontinent; NIP: Northern Indian Protocontinent; SLK: Sri Lanka; LCP: Laccadive Plateau; ATTC: Alleppey-Trivandrum Terrace Complex; NMR: Northern Madagascar Ridge; SEY: Seychelles Plateau; LAX: Laxmi Ridge; SVP: Saurashtra Volcanic Platform.

Fig. 3: Map showing locations of selected sea-surface gravity, magnetic, and multibeam bathymetry profiles and seismic sections over the Raman Seamount, Panikkar Seamount and the Wadia Guyot (the extents are shown using isobaths of 250 m interval) in the axial part of the Laxmi Basin used in the present study. The grey-coloured region represents the extent of the Panikkar Ridge (PKR). LAX: Laxmi Ridge; MB: Multibeam Bathymetry; G: Free-air gravity profiles; M: Magnetic profiles

Fig. 4: High-resolution two-dimensional multibeam bathymetry maps depicting the geomorphology of (a) the Raman Seamount, (b) the Panikkar Seamount, and (c) the Wadia Guyot, and their adjacent regions complemented by global bathymetry data GEBCO 2021 in the background. S1, S2 and S3 represents Segment-1, Segment-2 and Segment-3 of the Panikkar Seamount.

Fig. 5: High-resolution three-dimensional multibeam bathymetry maps of (a) the Raman Seamount viewing at 135° azimuth and 36° elevation; (b) the Panikkar Seamount viewing at 120° azimuth and 40° elevation, and (c) the Wadia Guyot viewing at 210° azimuth and 40° elevation.

Fig. 6: Maps of the Raman Seamount, Panikkar Seamount and the Wadia Guyot obtained from various terrain analyses: (a-c) the slope maps, (d-f) the terrain aspect maps and (g-i) the terrain ruggedness maps. The colour scale used in (e) is the same for (d) and (f). R: Raman Seamount; P: Panikkar Seamount; W: Wadia Guyot

Fig. 7: Identified channel patterns from the high-resolution multibeam bathymetry data of (a) the Raman Seamount, (b) the Panikkar Seamount, and (c) the Wadia Guyot. The two-dimensional bathymetry map of the seamount is given in the background.

Fig. 8: Seismic reflection section (a) across the Raman Seamount, and (b) its interpreted version; the seismic reflection section (c) across the Panikkar Seamount, and (d) its interpreted version; and the seismic reflection section (e) across the Wadia Guyot (from profile RE-11, modified after Krishna et al. (2010)) and (f) the interpreted version. Locations of these sections are given in Fig. 3 as red lines. The interpretations for (b) and (d) were obtained from Srinivas (2004).

Fig. 9: The free-air gravity anomaly maps of (a) the Raman Seamount, (b) the Panikkar Seamount, and (c) the Wadia Guyot, with superimposed isobaths defining their bathymetric extent (isobaths of 100 m interval for Raman and Panikkar seamounts, and isobaths of 200 m interval for Wadia Guyot).

Fig. 10: The magnetic maps of (a) the Raman Seamount, (b) the Panikkar Seamount, and (c) the Wadia Guyot, with superimposed isobaths defining their bathymetric extent (isobaths of 100 m interval for Raman and Panikkar seamounts, and isobaths of 200 m interval for Wadia Guyot).

Fig. 11: (a) Updated magnetic isochron map of the study area prepared by using the magnetic anomaly picks derived from the present study, complemented by those available from Bhattacharya and Yatheesh (2015); (b) The revised magnetic anomaly picks and isochron map around the Raman Seamount and adjacent regions with superimposed bathymetry map of the seamount showing the relationship of the bathymetric extent of the Raman Seamount with the revised magnetic isochrons; (c) The revised magnetic anomaly picks and isochron map around the Panikkar Seamount with superimposed bathymetry map of the seamount showing the relationship of the bathymetric extent of the Panikkar Seamount with the revised magnetic isochrons.

Table Captions

Table 1: Morphometric details of the Raman Seamount, Panikkar Seamount and the Wadia Guyot derived from the multibeam bathymetry data used in the present study.

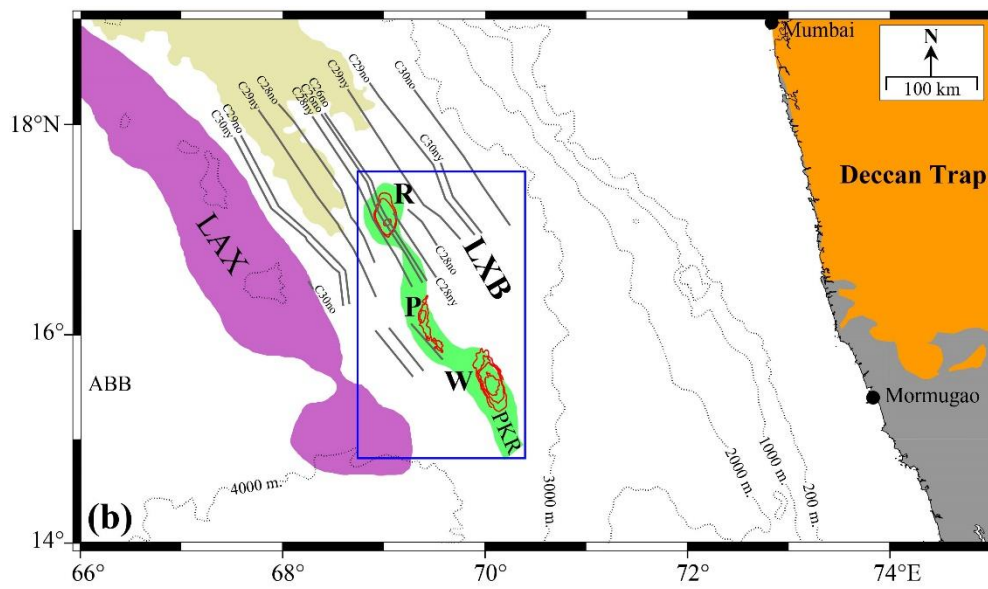
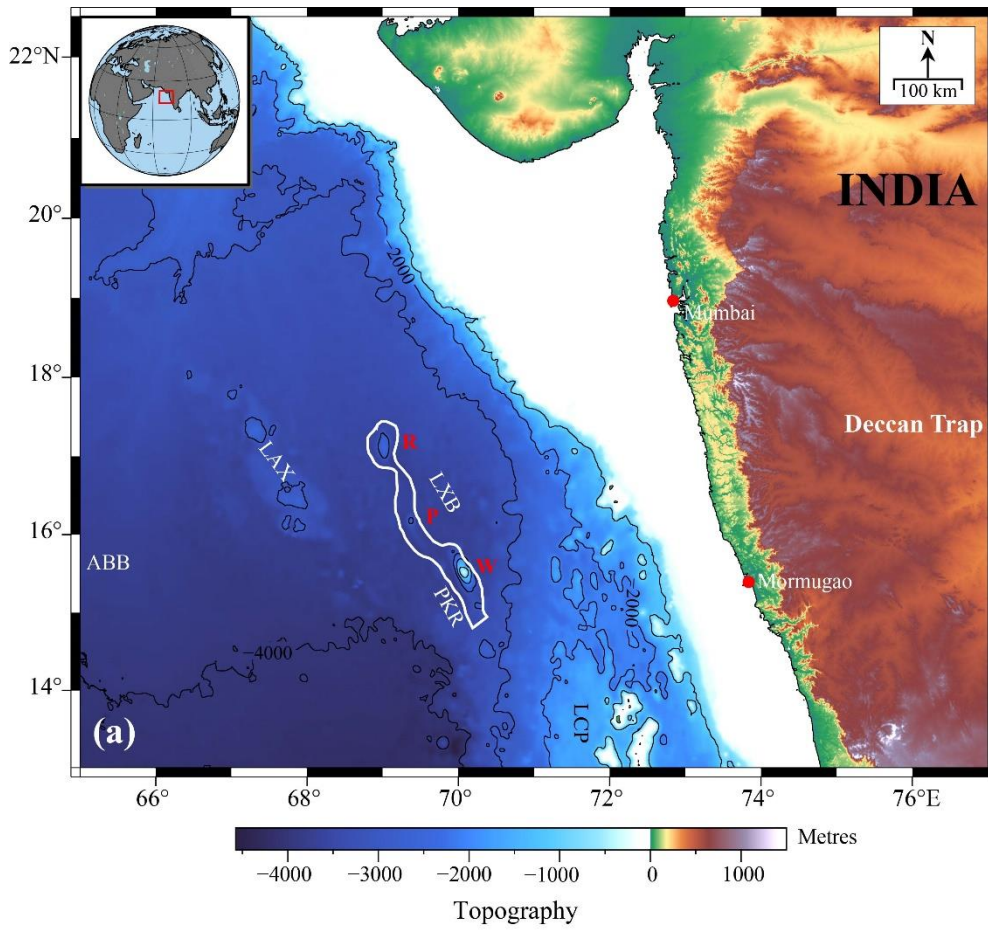


Figure 1

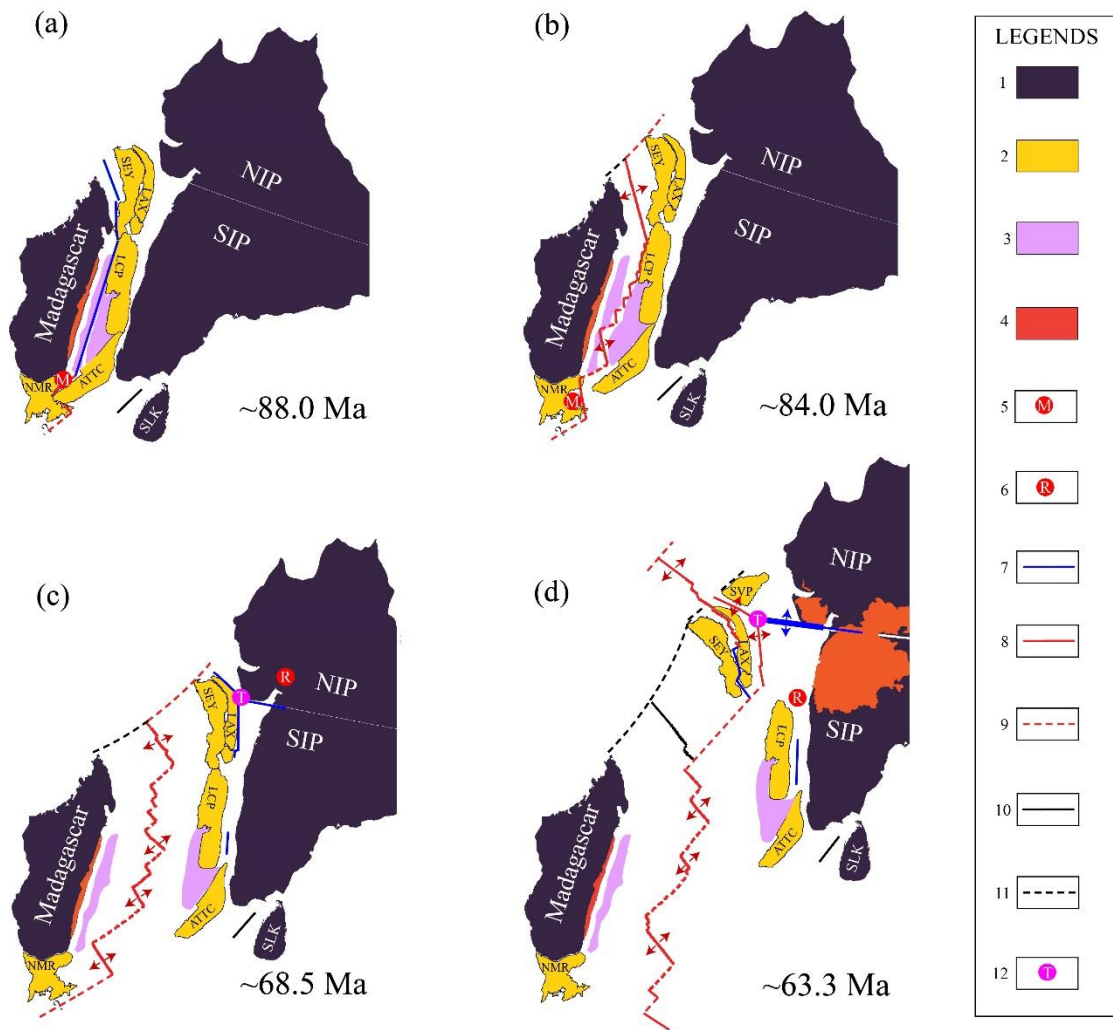


Figure 2

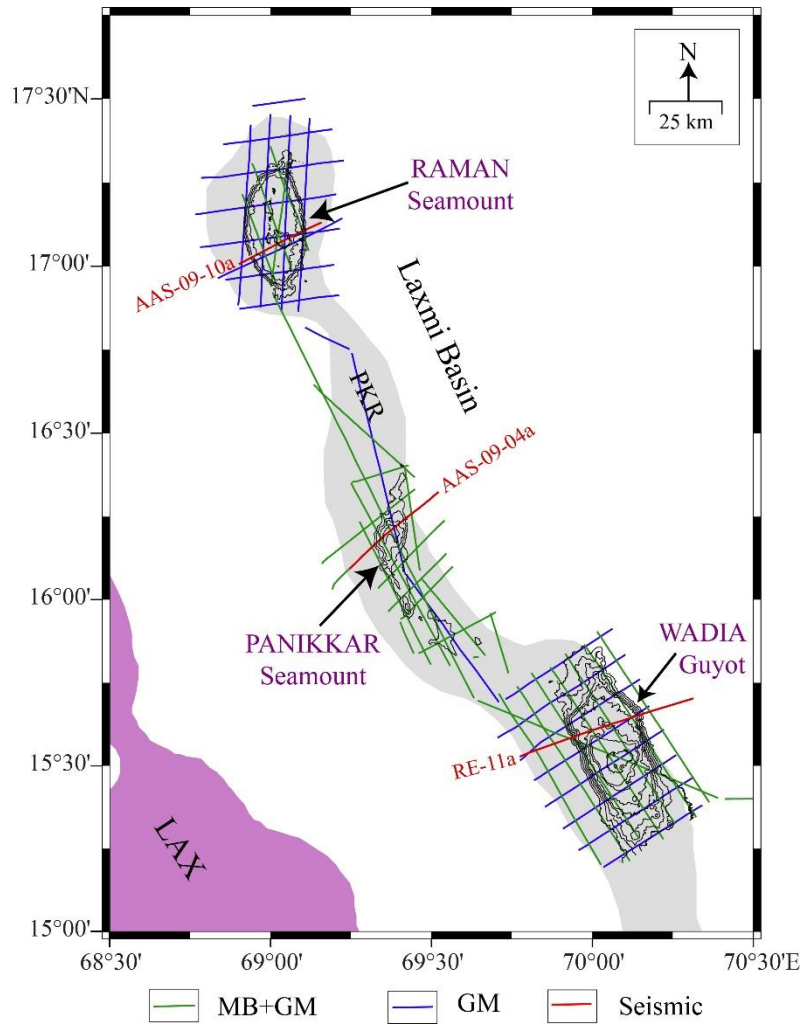


Figure 3

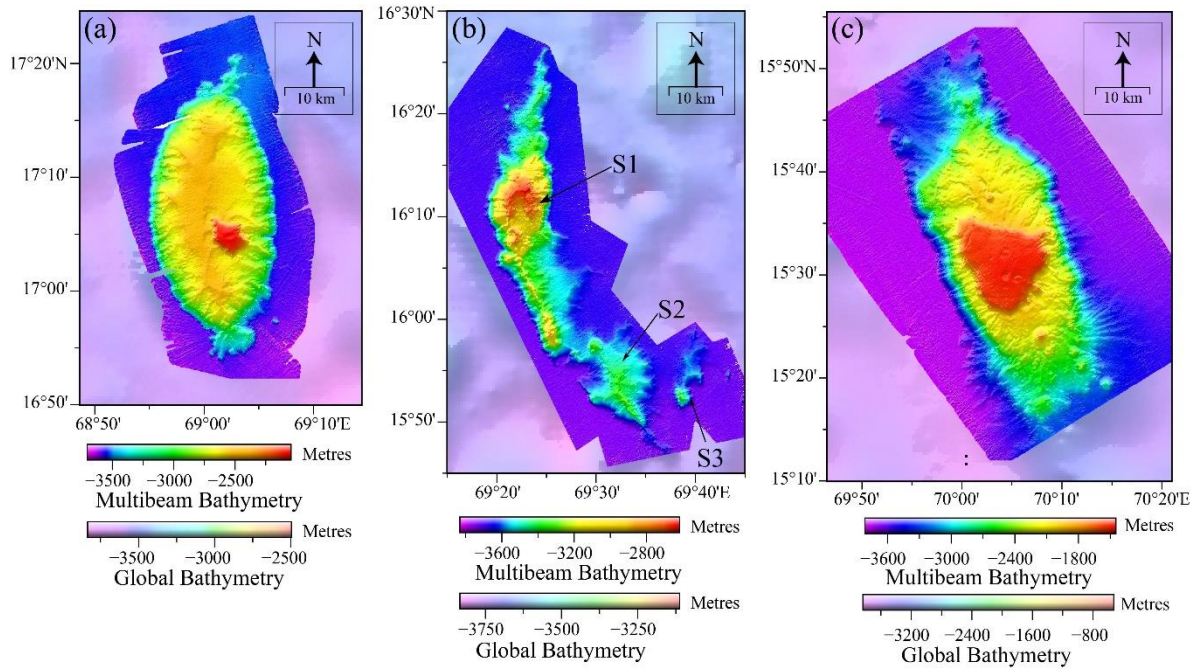


Figure 4

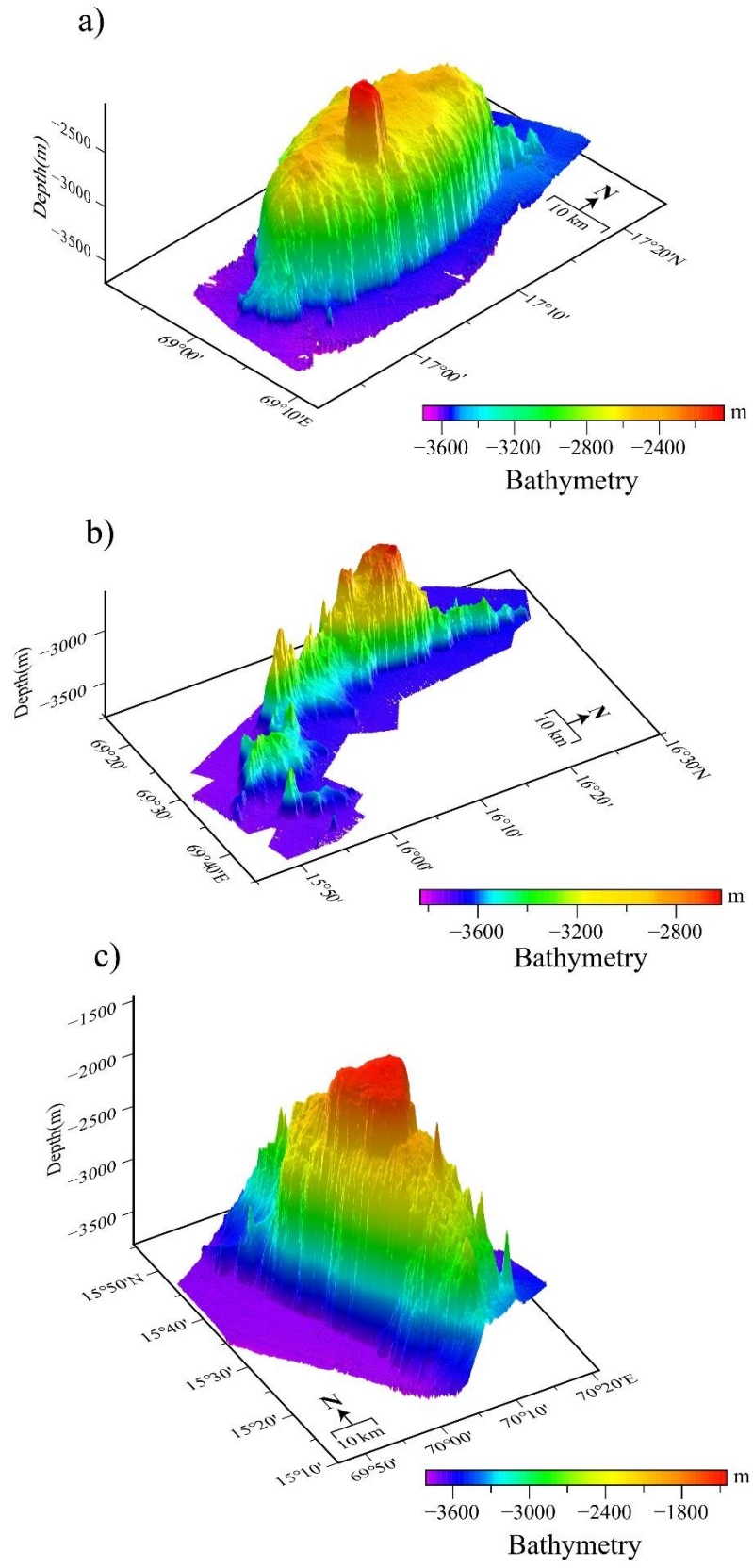


Figure 5

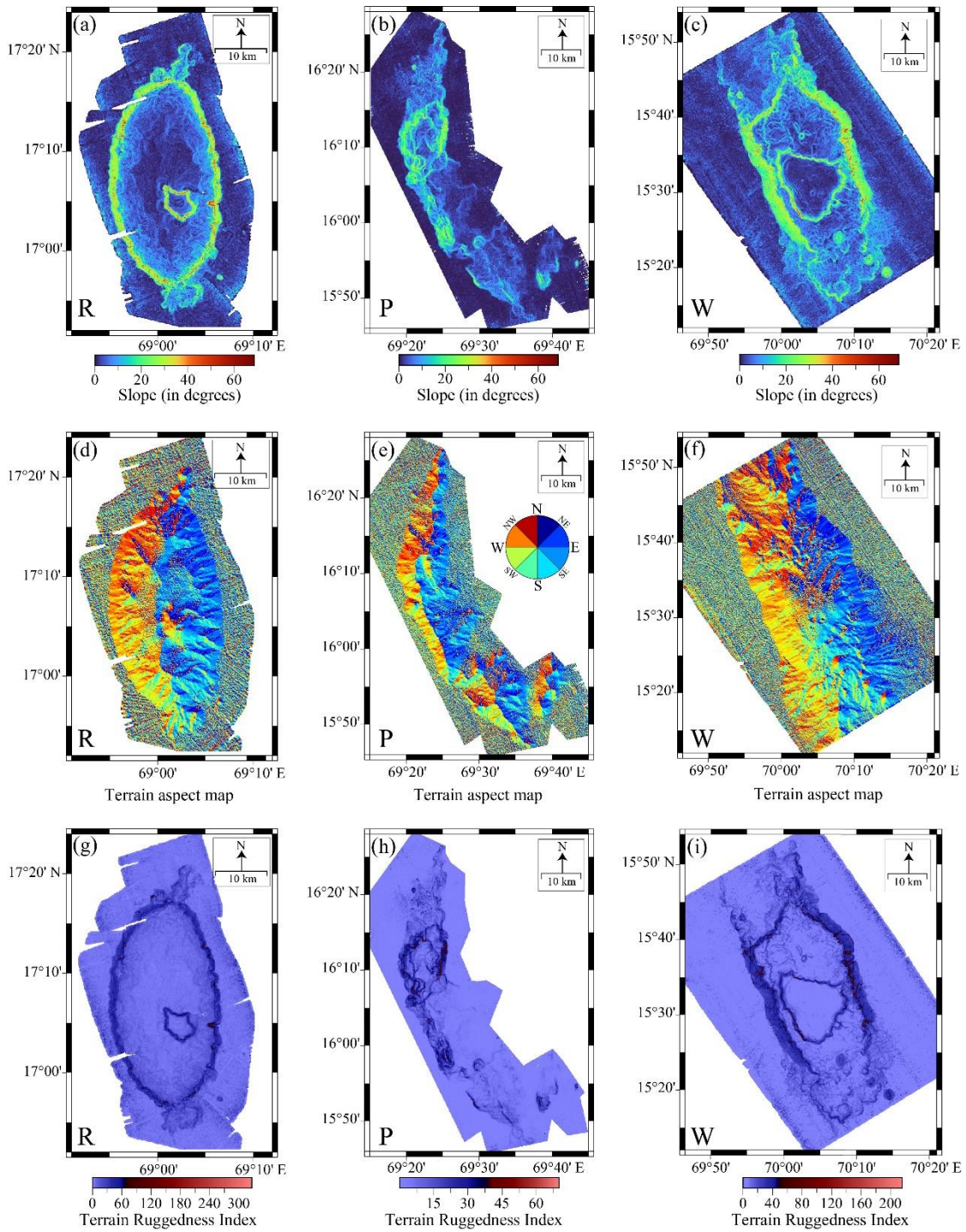


Figure 6

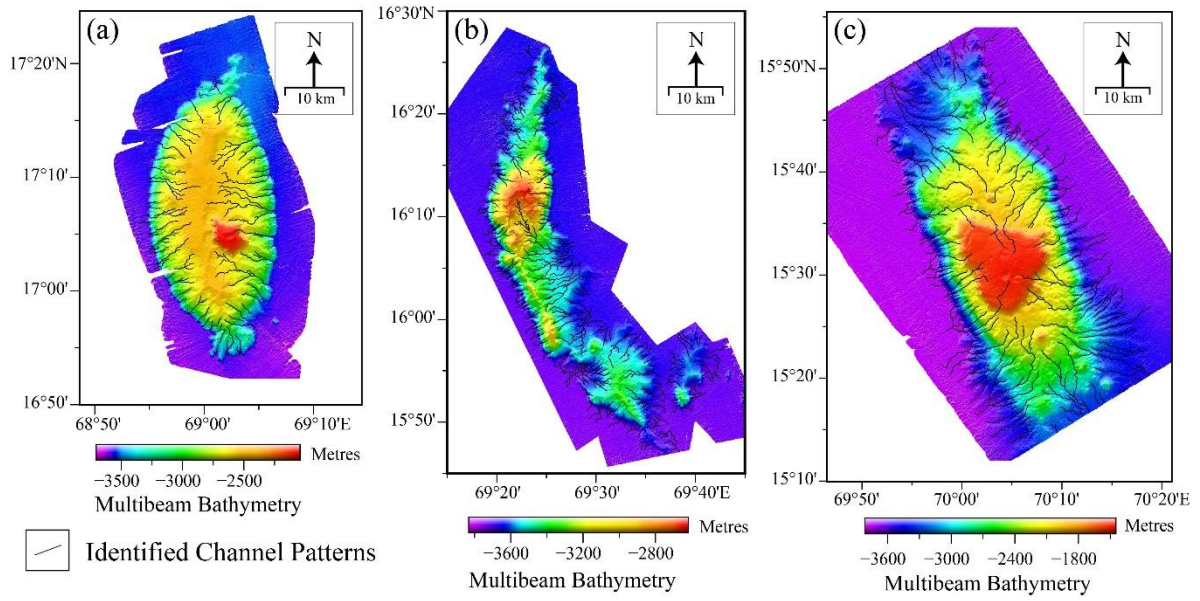


Figure 7

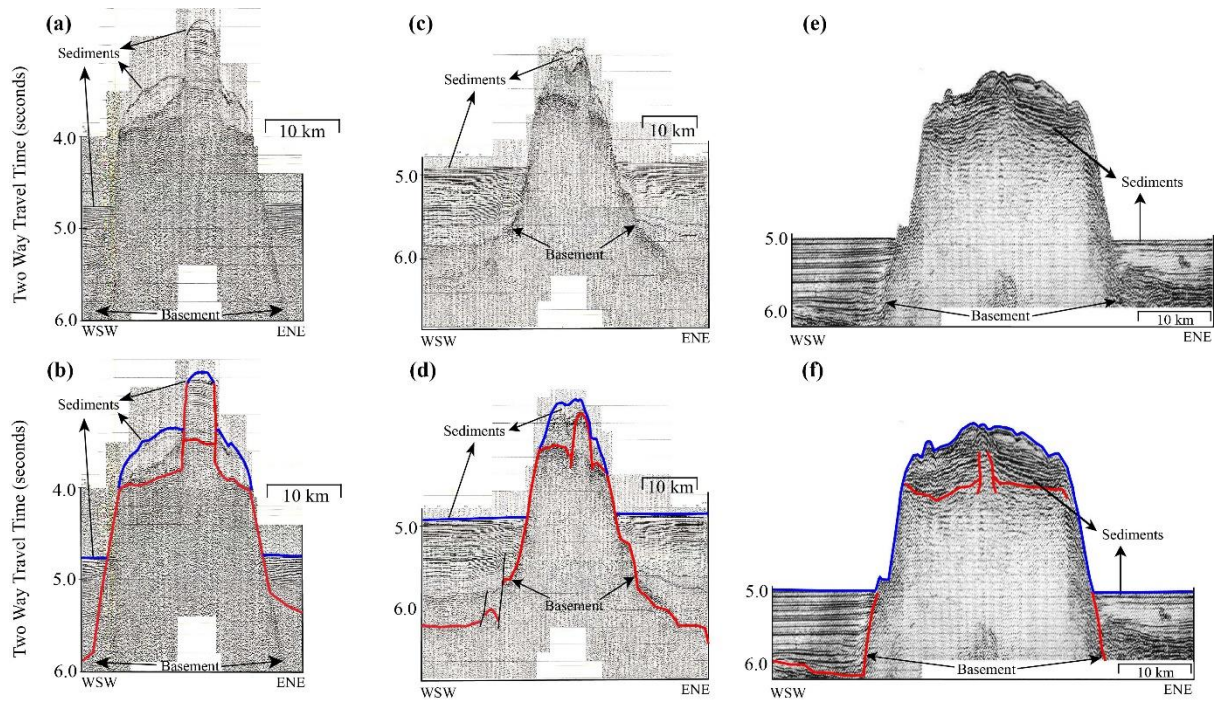


Figure 8

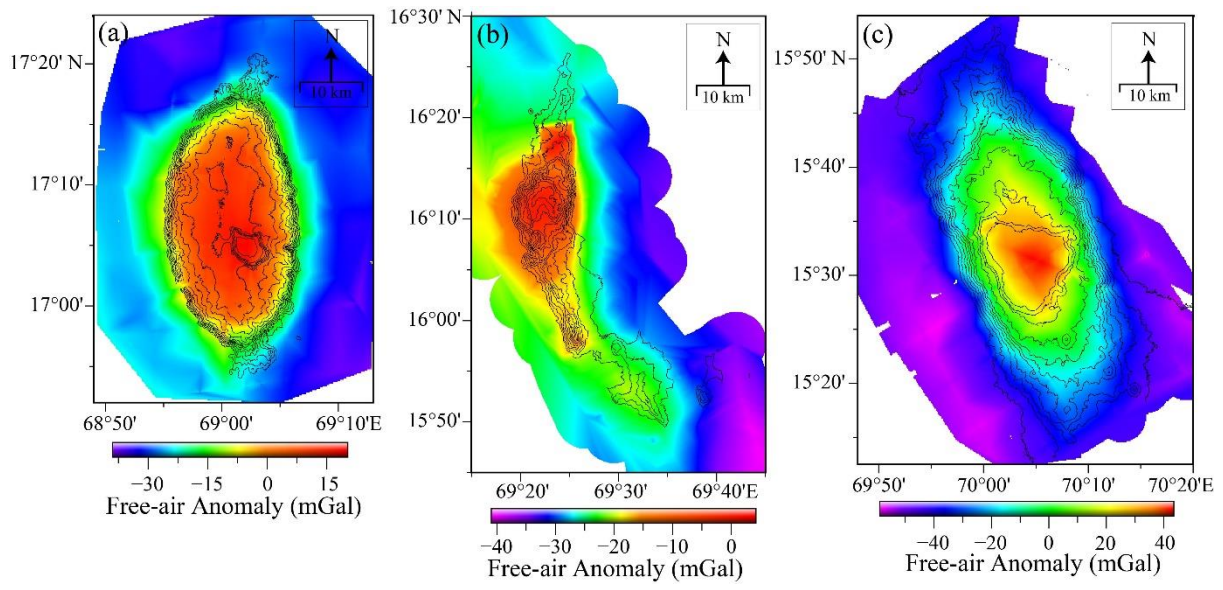


Figure 9

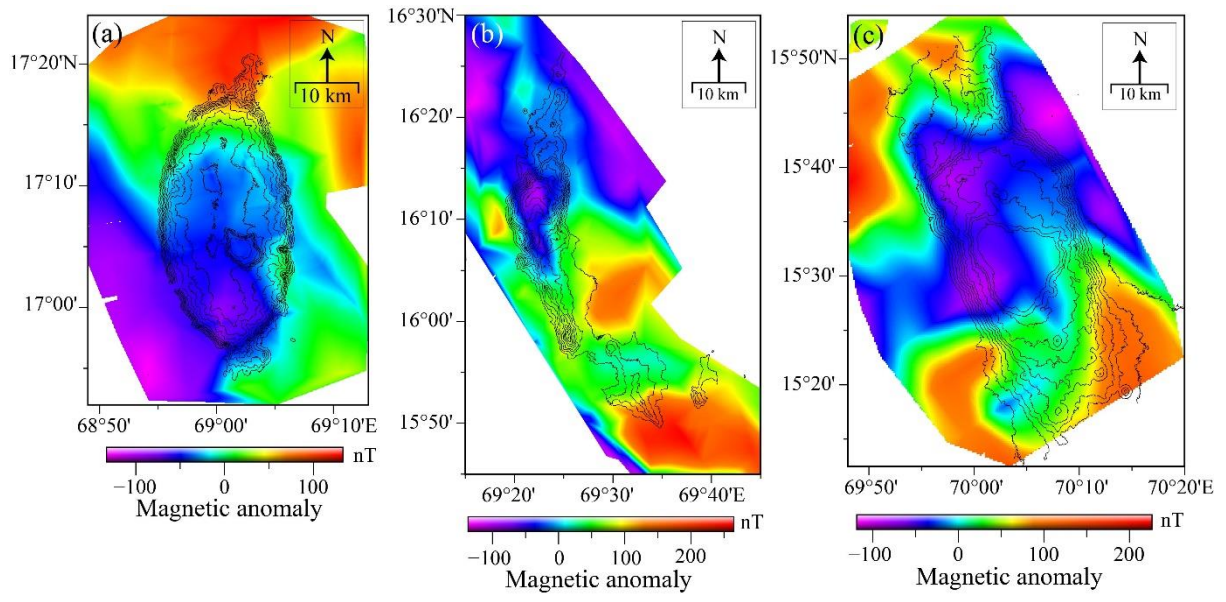


Figure 10

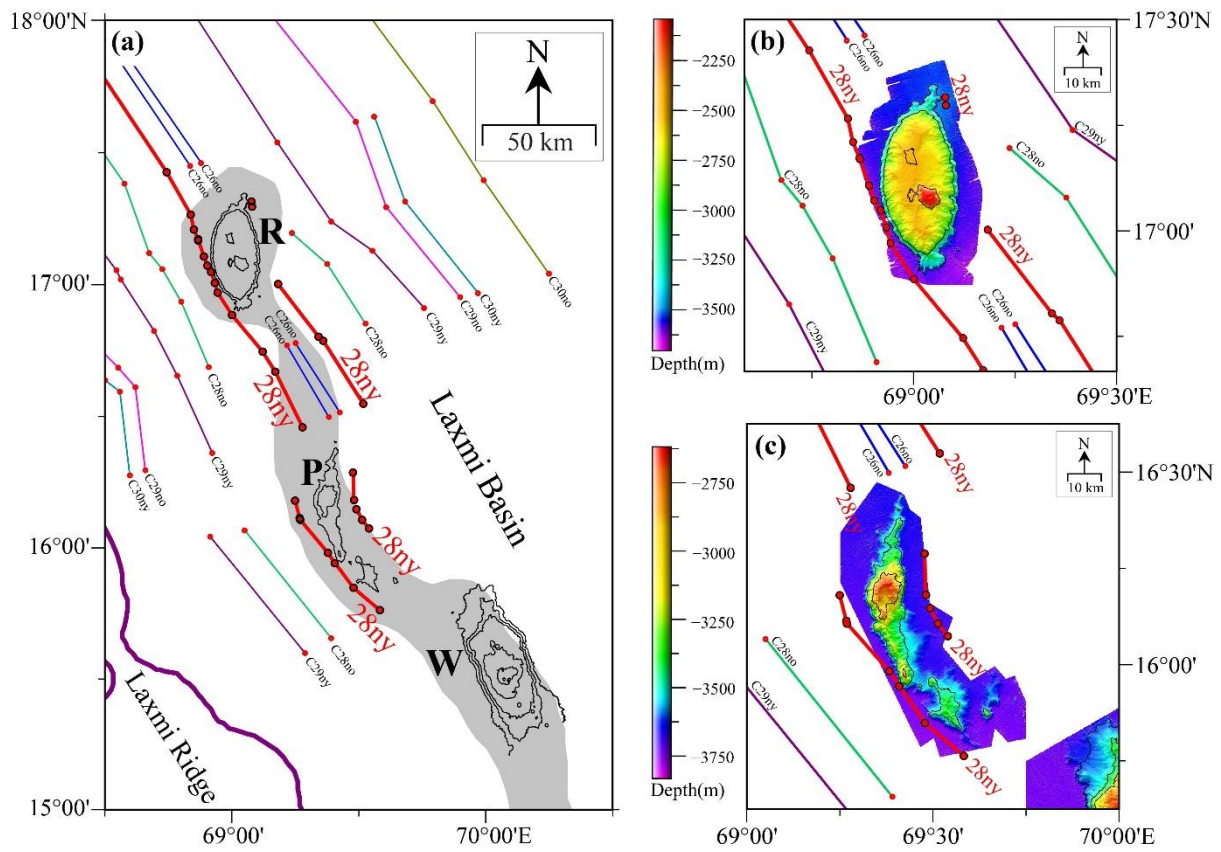


Figure 11

Table 1

Name of the Seamount	Location of the summit		Depth to the Summit	Reference depth to the base	Total height	Basal Area
	Longitude	Latitude				
Raman Seamount	69° 01.90' E	17° 05.05' N	~2042 m	~ 3550 m	~1508 m	~672 km ²
Panikkar Seamount	69° 23.12' E	16° 12.65' N	~2618 m	~ 3650 m	~1032 m	~560 km ²
Wadia Guyot	70° 04.39' E	15° 30.83' N	~1446 m	~ 3700 m	~2254 m	~1534 km ²